PROCEEDINGS, Thirty-Ninth Workshop on Geothermal Reservoir Engineering
Stanford University, Stanford, California, February 24-26, 2014
SGP-TR-202

Exploration Drilling and Technology Demonstration At Fort Bliss

Ben Barker[1], Joe Moore[2], Marylin Segall[2], Greg Nash[2], Stuart Simmons[2], Clay Jones[2], Jon Lear[3] and Carlon Bennett[3]

[1]237 Dartmouth Way, Windsor, CA 95492; [2]Energy & Geoscience Institute, Univ. of Utah, 423 Wakara Way, Ste. 300, Salt Lake City, UT 84108; [3]Ruby Mountain, Inc., 2373 East 1300 South, Salt Lake City, UT 84108

[1]geothermalben@gmail.com; [2]jmoore,mpsegall,gnash,ssimmons, cjones@egi.utah.edu; [3]rubymtn@aol.com, carlonbennett@gmail.com

Keywords: low enthalpy, Fort Bliss, Tularosa, Hueco, New Mexico,

ABSTRACT

The Tularosa-Hueco basin in south-central New Mexico has long been known as an extensional area of high heat flow. Much of the basin is within the Fort Bliss military reservation, which is an exceptionally high value customer for power independent of the regional electric grid and for direct use energy in building climate control. A series of slim holes drilled in the 1990s established the existence of a thermal anomaly but not its practical value. This study began in 2009 with a demonstration of new exploration drilling technology. The subsequent phases reported here delivered a useful well, comparative exploration data sets and encouragement for further development.

A production-size well, RMI56-5, was sited after extensive study of archival and newly collected data in 2010-2011. Most of 2012 was taken up with getting state and Federal authorities to agree on a lead agency for permitting purposes, getting a drilling permit and redesigning the drilling program to suit available equipment. In 2013 we drilled, logged and tested a 924 m well on the McGregor Range at Fort Bliss using a reverse circulation rig. Rig tests demonstrated commercial permeability and the well has a 7-inch slotted liner for use either in production or injection. An August 2013 survey of the completed well showed a temperature of 90 C with no reversal, the highest such temperature in the vicinity. The well's proximity to demand suggests a potentially valuable resource for direct use heat and emergency power generation.

The drilling produced cuttings of excellent size and quality. These were subjected to traditional analyses (thin sections, XRD) and to the QEMScan™ for comparison. QEMScan™ technology includes algorithms for determining such properties of rocks as density, mineralogy, heavy/light atoms, and porosity to be compared with direct measurements of the cuttings. In addition to a complete cuttings set, conventional and resistivity image logs were obtained in the open hole before the well was cased.

1. INTRODUCTION

The White Sands Missile Test Range and Fort Bliss are the first and second largest U.S. Army bases, together covering more than 10 000 km^2 of southeastern New Mexico. Although Fort Bliss is headquartered in El Paso, Texas, its principal training area is 2 400 km^2 in the southeast corner of Otero County, New Mexico designated as the McGregor Range (Figure 1).

Figure 1: Location of McGregor Range

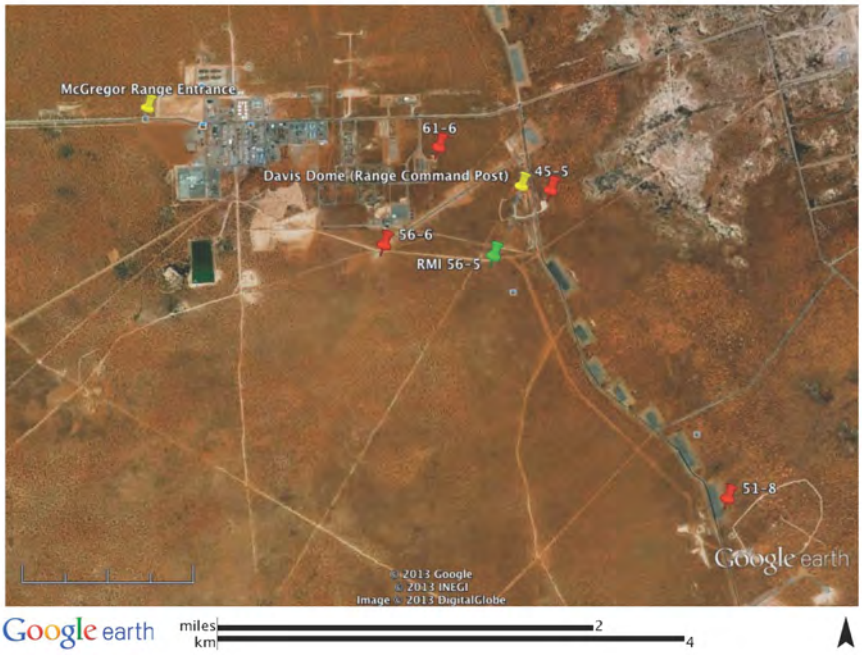

Figure 2: Area of McGregor Range Command Post and wells

The El Paso County Geothermal Project at Fort Bliss is a project is funded with a grant from the United States Department of Energy (DOE) as part of the American Recovery and Reinvestment Act of 2009. The project is administered through the DOE Golden Field Office to El Paso County, Texas. El Paso County includes the city of El Paso and is engaged with the U.S Army in developing the accommodations and services needed to support the ongoing major expansion of Fort Bliss. The primary subcontractor to El Paso County and the project's Principal Investigator, Ruby Mountain Inc. (RMI), assembled the project team consisting of Evergreen Clean Energy Management (ECEM) and the Energy & Geoscience Institute (EGI) at the University of Utah.

The El Paso County Geothermal Project at Fort Bliss is focused primarily on the McGregor Range area in an effort to determine the scale and utility of its geothermal resources. Previous workers identified this as an area of elevated heat flow and Sandia confirmed temperatures in the 80-85 C range through slim hole (wireline core) drilling but found little permeability (Finger and Jacobson, 1997). The initial project phase in 2010-11 included collecting and assessing all existing literature and data as well as conducting limited field testing of the four slim holes on the McGregor Range (Figure 2). At the conclusion of this early work the project team concluded that the older slim holes provided enough evidence of a convective geothermal regime in the 90 C range and no additional slim hole drilling would be worthwhile.

With the concurrence of DOE and Fort Bliss, the project was redirected to drilling a well of sufficient size and depth to allow for flow testing the geothermal resource. The project geoscientists at EGI identified suitable well sites and RMI worked to obtain permits. After a year of dealing with institutional issues, Fort Bliss received a permit for well RMI 56-5 from the New Mexico State Engineer. The rig commenced work under ECEM direction on May 17, 2013 and completed the well on June 28, 2013 at a total depth of 924 m.

2. DRILLING SUMMARY

Site selection was based on a combination of factors, principally temperature, expected fracture density and staying out of the way of Army operations. Fracture density was especially critical in light of the low permeabilities observed by Sandia. The site of RMI 56-5 was selected near a mapped fault intersection and down-drainage from an adjacent tank trail, to minimize the risk of a water release. In the event, there were no noteworthy incidents or spills and the cooperation of McGregor Range management was outstanding.

The four slim holes drilled in 1997 all experienced severe loss of circulation which the core rig could tolerate. In order to drill a larger diameter well in the same conditions the reverse circulation method was used. The drillers were sufficiently experienced and confident in this technology that ECEM was able to negotiate a hybrid footage-hourly contract that mitigated the project's exposure to variations in penetration rate enough to proceed with a very tight budget. This was an efficient structure that allowed the same contractor to deliver RMI 56-5 for a lower cost per meter (in 2013 dollars) than they had in 1997 using a continuous coring rig. Well RMI 56-5 Completion:

508 mm (20 inch) conductor cemented surface to 12.5 m (41 ft)

340 mm (13.375 inch) casing cemented surface to 176.5 m (579 ft)

178 mm (7 inch) slotted liner standing from 146.5 m (480 ft) to 920 m (3017 ft) in 222 mm (8.75 inch) OH

3. GEOLOGY

The Tularosa basin (Fig. 3) is a graben located in the southern Rio Grande Rift. The McGregor geothermal system lies on the eastern margin of the Tularosa-Hueco basin in south-central New Mexico near the border of Texas (Fig. 1). This area has a complex tectonic history beginning with Paleozoic siliciclastic sedimentation on a once low-lying shelf of the North American Craton. This was followed by periods of crustal shortening, including Late Paleozoic deformation related to Ancestral Rocky Mountains uplift and the Late Cretaceous Laramide Orogeny. The current landscape has been shaped by extensional tectonics, with the resultant development of the Rio Grande Rift. Extension began in the Late Paleogene and is accompanied by high heat flow. However, seismic activity is infrequent, relative to that in the Great Basin to the northwest, indicating that extension may be slowing in this area.

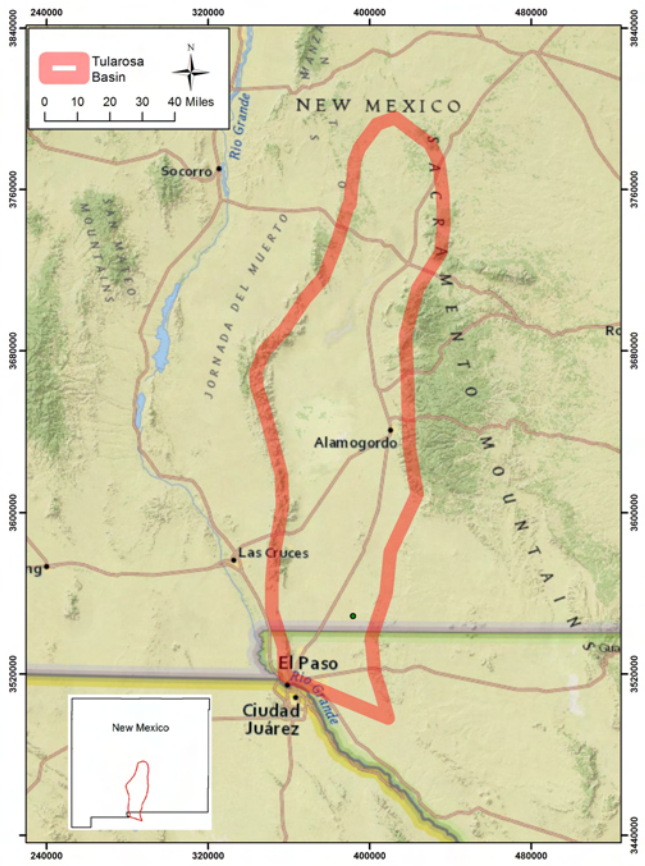

Figure 3: The Tularosa Basin lies in southern New Mexico and extreme western Texas in the southernmost part of the Rio Grande Rift

The fault-controlled deep-circulation McGregor system occurs within a small intra-bolson horst, known as Davis Dome, which is partially covered by basin fill. Several geophysical surveys have been undertaken in this area, including gravity, seismic, self-potential, and resistivity, to better characterize the geologic structure and the geothermal system. Fault and hydrothermal mineralogy mapping, from ASTER multispectral satellite imagery analysis, augments this data. Temperature surveys were also completed to assess heat flow and to locate thermal anomalies and a soil mercury survey was done to locate anomalous mercury accumulations that may be related to geothermal system degassing. Additionally, four deep slim-holes (46-6, 45-5, 61-6, and 51-8, Figure 2) provided additional temperature and geochemical data, including Geothermometers, which led to sitting the location for RMI 56-5.

The confirmation well (RMI 56-5) penetrated basin fill, Pennsylvanian limestone, felsite intrusions, Mississippian limestone interbedded with shale, and Silurian dolostone. The mudlog indicates that the well crosses significant fault zones at about 113 m and 393 m depth. Temperature profiles in well 45-5 (Fig. 4), which lies to the NNE of 56-5, suggest that this well may have intersected the same fault as RMI 56-5, but at shallower depth, as it heats up rapidly and then goes isothermal within the first few hundred feet of depth.

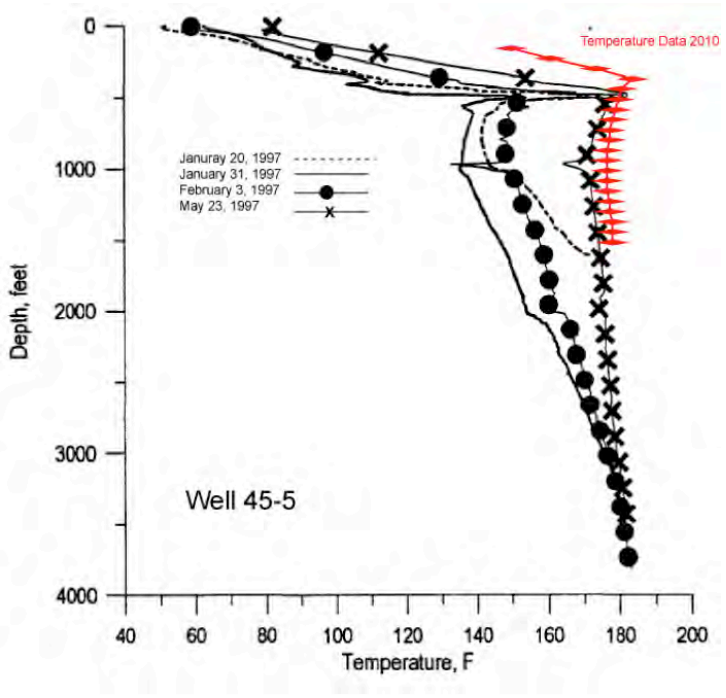

Figure 4: Well 45-5 temperature profiles

4. GEOCHEMISTRY

Thermal water compositions were analyzed from three separate sampling campaigns in 1997, 2011, and 2013 (Table 1), and they comprise dilute (<1 wt % TDS), near neutral pH solutions. The 2011 samples in Table 1 were collected by bailer, as is noted for most of the 1997 samples. The 2013 samples from RMI 56-5 were collected with a downhole sampler on electric line six weeks after completion.

The dominant anion is chloride, with lesser sulfate and bicarbonate (Fig. 5). Sodium is the dominant cation followed in order of decreasing concentration by calcium, potassium and magnesium. The silica concentrations are low (<75 mg/kg SiO2), and fluoride, boron, and lithium comprise minor constituents. These compositions are typical of waters found in marine sedimentary sequences strongly influenced by interaction with limestones.

The completion of well RMI 56-5 and the acquisition of new water analyses (2013) permit further characterization of the reservoir composition and an assessment of the state of fluid-mineral equilibria. The shallower water sample from 381 m is associated with a fault zone that transects a thick sequence of limestone. The deeper water sample from 902 m coincides with the stratigraphic contact between shale and felsite.

Table 1: Water analyses from Ft. Bliss wells (mg/kg)

Sample Name	Depth (ft)	T °C	pH	Li	Na	K	Ca	Mg	SiO_2	B	Cl	F	SO_4	HCO_3
1997														
45-5 485 ft bailed	485	85	7.48	1.41	2010	96.2	258	44.8	32.3	1.06	3279	2.87	665	177
45-5 588 ft bailed	588		7.67	0.29	562	26.5	102	18.3	33.2	0.28	909	1.08	179	132
45-5 3,006 ft swabbed (ave)	3006	80		2.06	3580	215	491	95.2	44.1	1.58	5525	3.4	1055	352
45-5 3,006 ft swabbed (ave)	3006	78		2.06	3620	215	494	97.9	38.7	1.54	5398	3.12	1058	338
45-5 3,135ft bailed	3135	83	6.8	2.05	3570	228	480	98.9	61.4	1.46	5298	3.49	1054	375
45-5 3,600 ft bailed	3600	84		1.73	3210	176	384	77.9	73.6	1.41	4989	2.75	964	471
46-6 775 ft bailed	775	81	6.8	1.44	3710	125	361	59.4	59.7	1.49	4470	3.68	824	220
46-6 1,337 ft bailed	1337	81		1.37	2650	116	327	53.7	33	1.51	4363	3.37	794	190
2011														
45-5				0.81	1945	91.8	6	1.22	3.96	1.59	2191	3.66	636	305
46-6				0.44	1051	58.9	584	0.366	0.85	0.63	2550	0.8	350	48
51-8				0.48	269	17.1	66.6	14.15	1.58	3.91	493	0.75	66.3	48.8
61-6				0.2	754	24.4	10	0.85	6.72	0.27	666	1.51	2393	461
2013														
56-5	1250	86	6.49	1.21	2680	117	305	51.7	41.8	1.36	4220	4.42	846	173
56-5	2960	93	7.06	1.23	2600	118	371	52.2	18.5	1.35	4270	3.97	834	309

Trilinear graphs show the relative proportions of Cl-HCO3-SO4 (Fig. 5) and Cl-B-HCO3 (Fig. 6). In both graphs, most of the waters form a coherent pattern and plot on simple linear trends, having Cl/SO4~5 and Cl/B~3500. These trends reflect dilution as is evident from binary plots in Figure 7. The 2011 data are the exceptions; along with their very low silica concentrations, they appear to be defective, and they are omitted from further discussion. The least diluted waters include 45-5 (1997), 46-6 (1997), and 56-5 (2013), which seem to best represent the reservoir fluid.

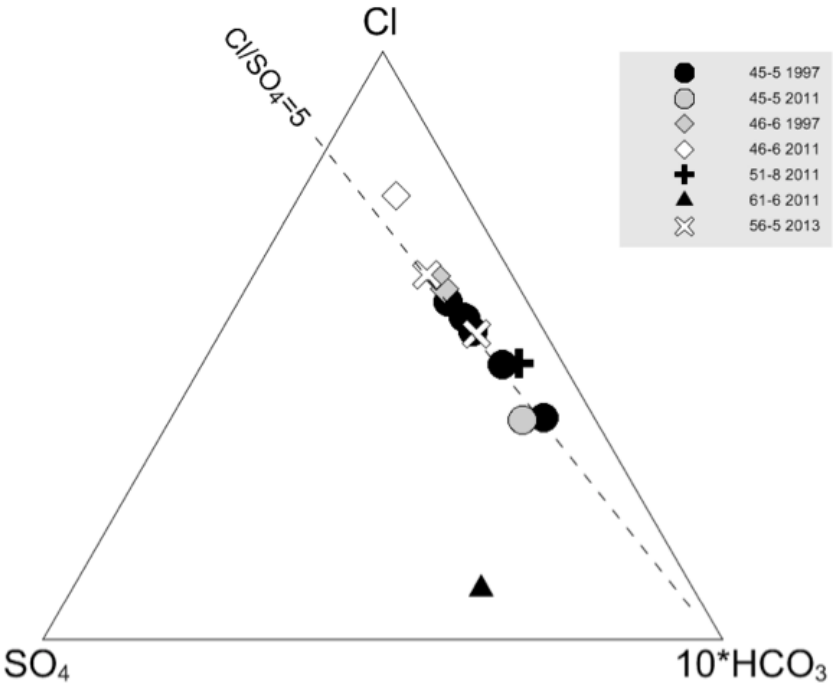

Figure 5: Cl-HCO3-SO4 trilinear graph of thermal water compositions

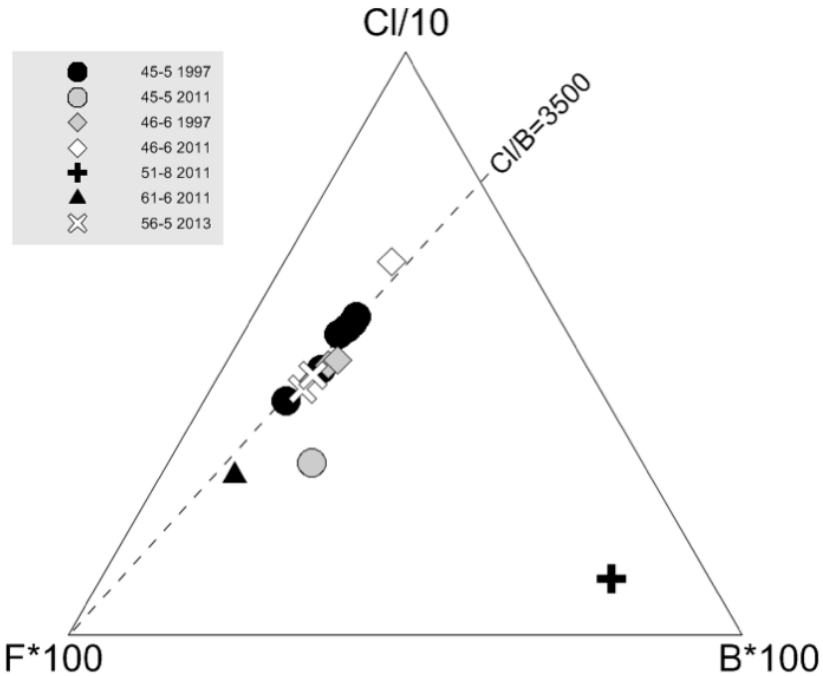

Figure 6: Cl-B-F trilinear graph of thermal water compositions

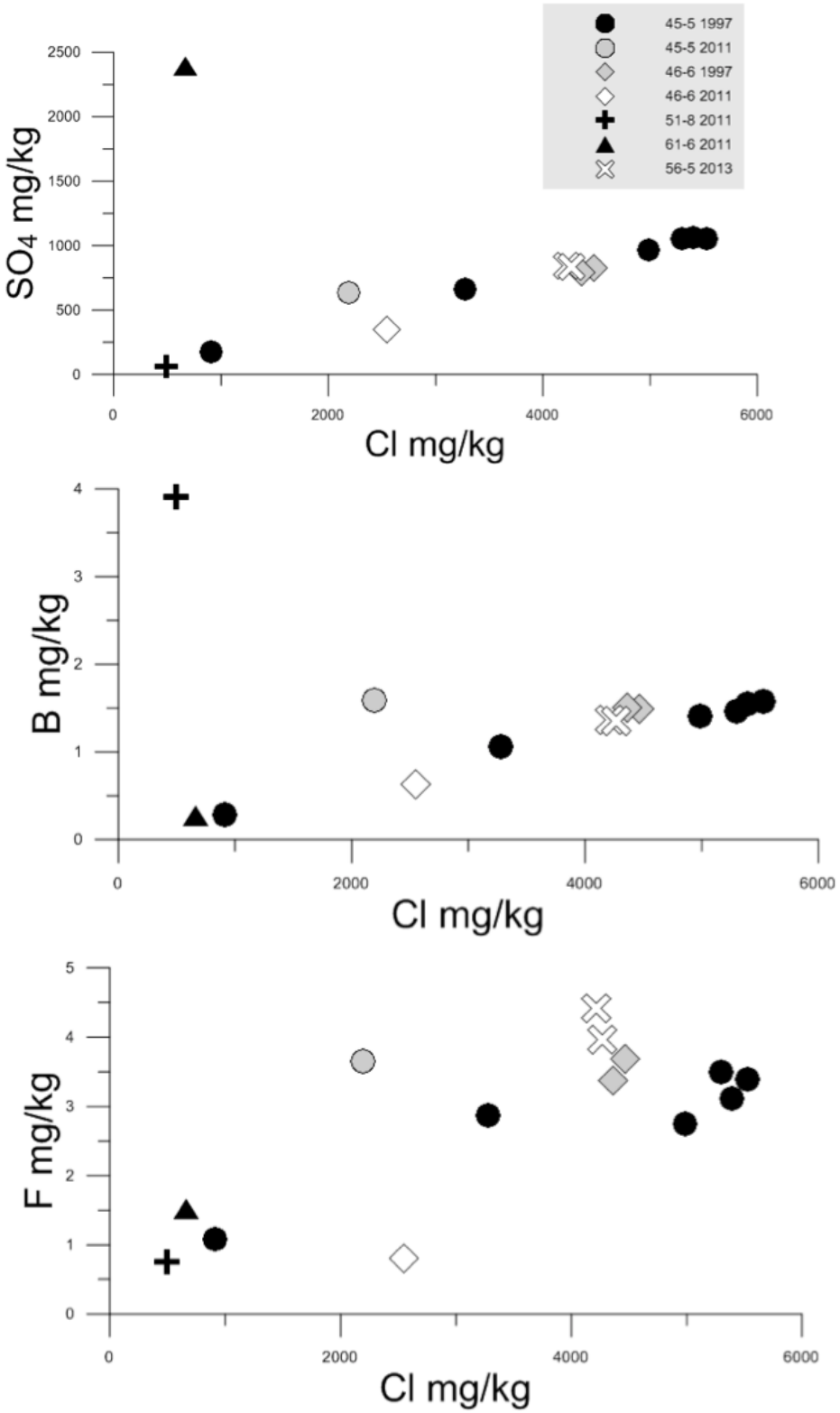

Figure 7: Binary plots (Cl vs SO4, Cl vs B, and Cl vs F) of thermal water compositions

Calculated equilibration temperatures using conventional chemical geothermometers are listed in Table 2. The quartz-silica (conductive) and chalcedony-silica temperatures most closely match measured temperatures except for RMI 56-5 at 902 m, and the low silica in this sample relative to the other waters is not easily explained. The Na-K equilibration temperatures are 80->100 C hotter than measured temperatures, showing this chemical geothermometer is unreliable. The K-Mg equilibration temperatures also exceed measured temperatures by 20-30 C, suggesting this chemical geothermometer is unreliable too.

Table 2: Equilibration temperatures (T °C) using conventional chemical geothermometers (Fournier, 1991; Giggenbach, 1991)

Sample Name	Tquartz	T chalcedony	T_{NK}	T_{KMg}
1997				
45-5 485'	83	51	180	104
45-5 588'	84	53	179	82
45-5 3006'	96	66	195	117
45-5 3006'	90	60	194	116
45-5 3135'	112	83	199	118
45-5 3600'	121	93	189	114
46-6 775'	110	81	158	108
46-6 1337'	84	52	174	107
2013				
56-5	94	63	174	108
56-5	61	29	176	108

The compositions of waters obtained from RMI 56-5, representing the hottest reservoir conditions, were further evaluated using SOLVEQ (Reed and Spycher, 2006). This software is used to calculate the distribution of aqueous species, which provides pH and mineral saturation indices at reservoir conditions (Table 3). The shallower water (381 m) is close to quartz saturation, which explains the match between measured and quartz equilibration temperatures; this water is also supersaturated in barite but undersaturated in calcite. The deeper water (902 m) is undersaturated in quartz and barite, but supersaturated in calcite. Both waters are undersaturated in fluorite and anhydrite. By numerically heating the deep water, anhydrite was found to reach saturation at 113 C, which conceivably represents a deep equilibration temperature if anhydrite exists in the sequence.

Table 3: Chemical attributes of the reservoir liquid; mineral saturation indices (Log Q/K) and pH were computed with SOLVEQ, with mineral saturation = 0.0, mineral undersaturation <0, and mineral supersaturation >0

Sample Name	Depth (ft)	T °C	pH	Quartz	Calcite	Fluorite	Anhydrite	Barite
56-5	1250	86	6.41	0.08	-0.19	-0.42	-0.39	0.19
56-5	2960	93	6.96	-0.35	0.88	-0.45	-0.24	-0.27

5. CUTTINGS ANALYSIS

5.1 X-Ray Diffraction Analysis

Table 4 illustrates the compositions of representative lithologies encountered in well RMI 56-5. The sedimentary sequence in the upper part of the well consists of calcareous sandstone and fossiliferous limestone that is cut by porphyritic granitic dikes. The granite porphyry contains resorbed quartz, plagioclase and minor hornblende and biotite phenocrysts in a micropoikilitic groundmass of plagioclase, K-feldspar and quartz (Figure 8). Plagioclase has been partially altered to carbonate, illite, K-feldspar and kaolinite. Hornblende and biotite have been completely altered to calcite, illite and opaque minerals. The granite is intensely sheared and altered at near its base. Veins are filled with quartz and carbonate. The deepest lithology observed is a fine-grained carbonate mudstone cut by veins of carbonate and chalcedony (Figure 8).

The distribution of the sheet silicates varies with depth. Smectite occurs in the upper part of the wells. It is the characteristic clay mineral at temperatures below about 180 C. Interlayered illite/smectite, which is indicative of temperatures between 180 and 225 C is common at intermediate depths. Below 610 m, illite is the dominant sheet silicate with lesser kaolinite and chlorite, although traces of smectite are present. Illite indicates temperatures exceeding 225 C (Henley and Ellis, 1983; Reyes, 1990). No epidote, a common high-temperature mineral (>250 C) was observed. The distribution of these mineral suggests temperatures during hydrothermal alteration were significantly higher in the past but did not exceed 250 C within the drilled portion of the system.

Table 4. Results of X-ray diffraction analyses with abundances given in weight percent. Tr indicates trace amounts are present (e.g. <1 weight percent). Lithologic abbreviation used; Ss, sandstone; Ls, limestone; G, granite and m, mudstone.

Depth ft	Lithology	smectite	interlayered illite/smectite	% illite in I/S	illite	chlorite	kaolinite	quartz	plagioclase	K-feldspar	calcite	dolomite	Siderite	pyrite
50-60	Ss	1			Tr		Tr	75	10	4	11			
200-210	Ss	7			5		3	48	11	16	12			
420-430	Ss		17	>90%		Tr	Tr	48			34			
600-610	Ls		Tr	<50%	Tr	4		13	1		74	7		Tr
770-780	Ls							7			93			
1000-1010	G	Tr			7		2	44	21	24	2			
1200-1210	Ls							4			96			
1400-1410	Ls					Tr		7			93			
1600-1610	Ls		6	>90%		8		20			66			Tr
1790-1800	Ss					Tr		75			25			
2000-2010	G	Tr			4		3	32	33	25	3			
2200-2210	G				5		1	31	36	24	3			
2400-2410	G	Tr			3		2	27	48	19	2			
2600-2610	G	Tr			4		3	35	37	18	Tr		3	
2800-2810	G	Tr			5		2	18	30	14	1	22	7	
2990-3000	m				20	10		36		24	6			5

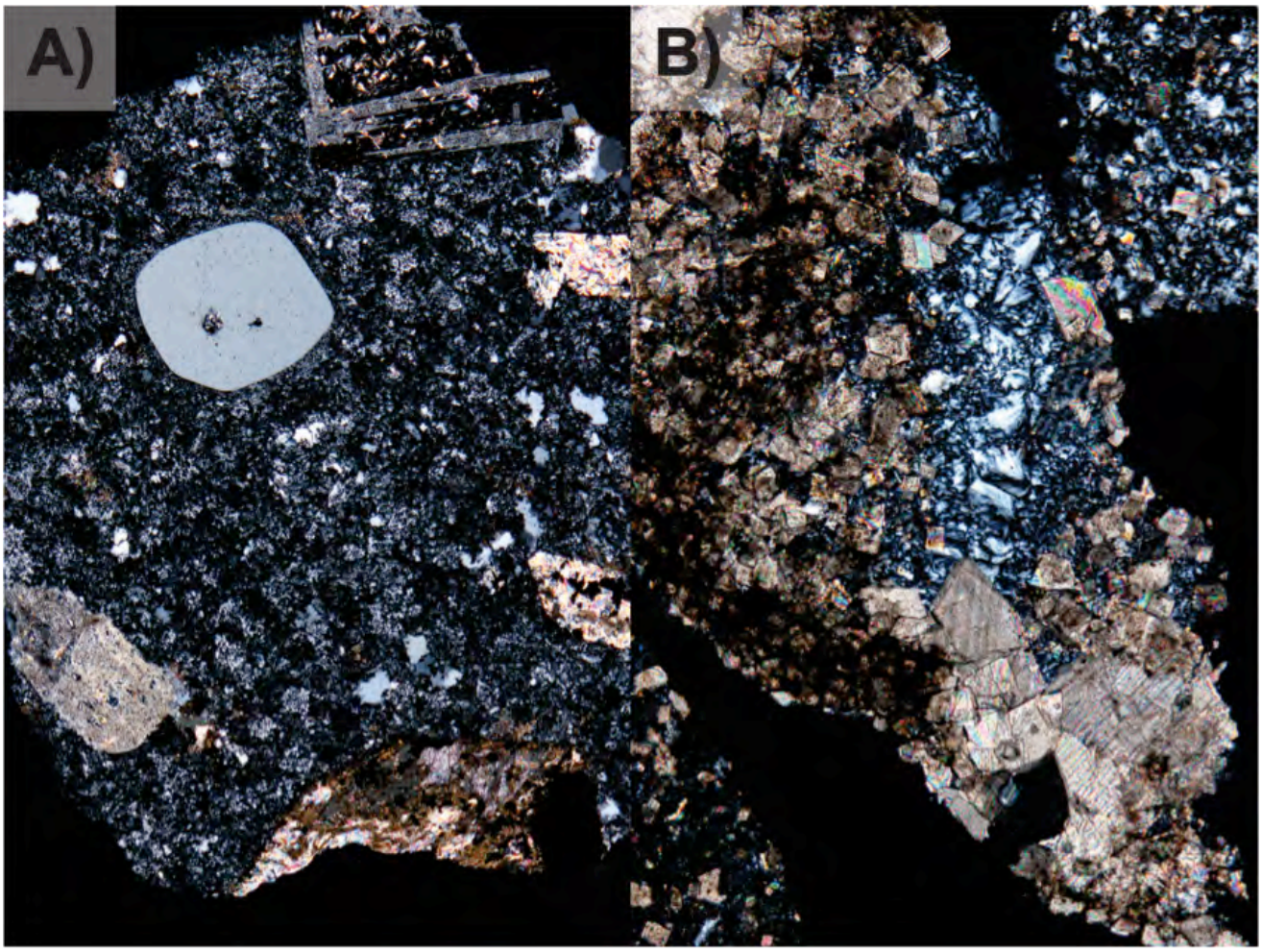

Figure 8: A) Granite porphyry that contains resorbed quartz (rounded crystal), plagioclase (rectangular crystals) and hornblende (lower edge of chip) phenocrysts in a micropoikilitic groundmass of plagioclase, K-feldspar and quartz. Plagioclase has been partially altered to calcite and illite. Hornblende has been completely altered to calcite (2700-2710 ft). B) Carbonate mudstone cut by a vein filled first by carbonate with later chalcedony (3020-3030 ft). Both photomicrographs were taken with crossed nicols and have a vertical fields of view of 3.2 mm (a) and 1.6 mm (B)

5.2 QEMScan Analysis and X-Ray Diffraction Comparison

Well samples were prepared for comparative XRD and QEMScan analyses. In general the mineralogic trends for both techniques produced similar results. Seven lithologic zones are identified based on mineralogic variability downcore (Table 1). Three of these are very similar and represent a distinct source and alteration processes for units 1, 3 and 5 (Table 1). They are shown as depositional/diagenetic Unit 1 in Figure 1. Two depositional sequences interrupt the succession above 1800 feet in the well. These are listed as Units 2 and 4 in Table 1 and depicted as Unit 2 in Figure 1.

Quartz is the dominant mineral in Unit 1, whereas calcite dominates Unit 2 (Fig. 1). Intraparticle porosity observed with QEMScan technology consists of two types: dominantly fracture porosity in Unit 1 and dissolution porosity in Unit 2 (Fig. 2). Both fracture and dissolution porosity occur in lowermost Units 3-5. Ankerite abundance increases from Unit 3 to a maximum of almost 20 % in Unit 4, where it occurs with siderite, pyrite, and domomite, in what is predominantly a siliciclastic sequence (Fig. 3).

Table 5: XRD and QEMScan Comparison

	Bulk Mineralogy %													
Depth ft	smectite	interlayered illite/smectite	%illite in I/S	illite	chlorite	kaolinite	quartz	plagioclase	K-feldspar	calcite	dolomite	siderite	pyrite	Unit
50-60	1			Tr	Tr	8	18	4	13					
200-210	7			5	3	8	48	11	16	12				
420-430		7	>90%		Tr	7	48			34				
600-610		11	>90%	Tr	4		34	11		28	7		Tr	
770-780							7			93				
1000-1010	Tr			7		4	46	11	18	9				
1200-1210							4			96				
1400-1410					Tr		7			93				
1600-1610		6	>90%		8		40			46			Tr	
1790-1800					Tr		54			45				
2000-2010	Tr			4		1	32	8	6	3				
2200-2210				5		1	35	16	14	3				
2400-2410	Tr			3		2	37	16	13	2				
2600-2610	Tr			4		3	35	21	18	7		3		
2800-2810	Tr			5		2	38	24	14	3	3	7		
2960-3000														
2990-3000				20	10		35		24	6			5	
3020-3030														

	QEMScan Mineral Analyses												
	Illite	Smectites	Chlorite	Kaolinite	Quartz	Plagioclase	Alkali Feldspar	Calcite	Dolomite	Micrite	Ankerite	Pyrite	Unit
	9.6	0.4	1.7	0.0	36.8	6.9	5.4	27.0	0.1	11.0	0.1	0.0	
	20.3	2.1	4.7	0.1	31.0	13.0	6.2	7.3	0.0	5.4	0.0	0.0	
	19.1	0.4	0.9	0.0	27.2	3.7	0.1	34.1	0.2	9.6	0.3	0.0	
	0.2	0.0	0.0	0.0	4.5	0.5	0.0	87.1	7.6	17.4	0.0	0.1	
	0.0	0.0	0.0	0.0	4.6	0.1	0.0	87.2	0.1	3.0	0.1	0.0	
	27.7	0.1	0.6	0.7	44.6	6.6	9.9	0.3	0.0	0.1	0.0	0.0	
	0.6	0.0	0.0	0.0	1.3	0.0	0.0	94.1	0.1	0.8	0.1	0.0	
	0.4	0.0	0.0	0.0	3.8	0.2	0.0	89.1	0.1	8.4	0.1	0.0	
	3.5	0.0	0.0	0.0	11.3	1.2	0.0	78.1	0.1	16.1	0.0	0.3	
	0.7	0.1	0.2	0.1	69.8	0.5	0.6	19.5	0.5	5.9	0.3	0.0	
	27.9	0.4	0.3	1.9	45.7	10.1	11.8	1.5	0.1	0.5	0.4	0.3	
	22.2	0.3	0.3	1.9	41.1	11.8	12.9	1.4	0.3	0.6	0.3	0.4	
	13.5	0.2	0.2	0.4	27.2	4.0	2.0.8	0.9	0.2	0.3	0.4	0.3	
	17.0	0.8	1.3	3.3	35.0	20.4	8.4	0.0	0.5	0.1	2.4	0.3	
	13.4	0.2	0.4	1.3	20.5	17.1	9.7	0.5	1.9	0.7	29.4	0.4	
	19.4	0.6	0.6	0.0	35.8	1.0	4.1	0.8	13.4	5.4	0.2	2.2	
	24.7	0.2	1.3	0.0	15.9	0.2	0.3	0.4	1.1	3.0	0.2	1.3	
	0.4	0.0	0.0	0.0	68.1	0.0	0.4	3.5	19.4	3.9	0.0	0.2	

* Insignificant quantities (not shown) of glauconite, muscovite, biotite, siderite, and pyrite were identified

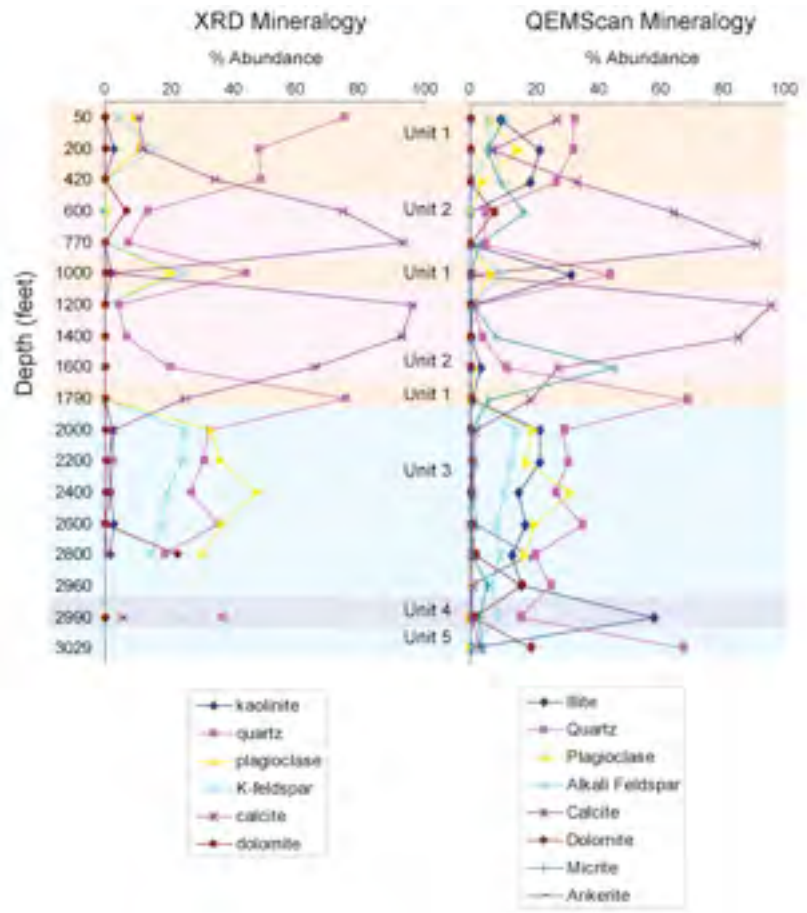

Figure 9: XRD and QEMScan Mineralogy

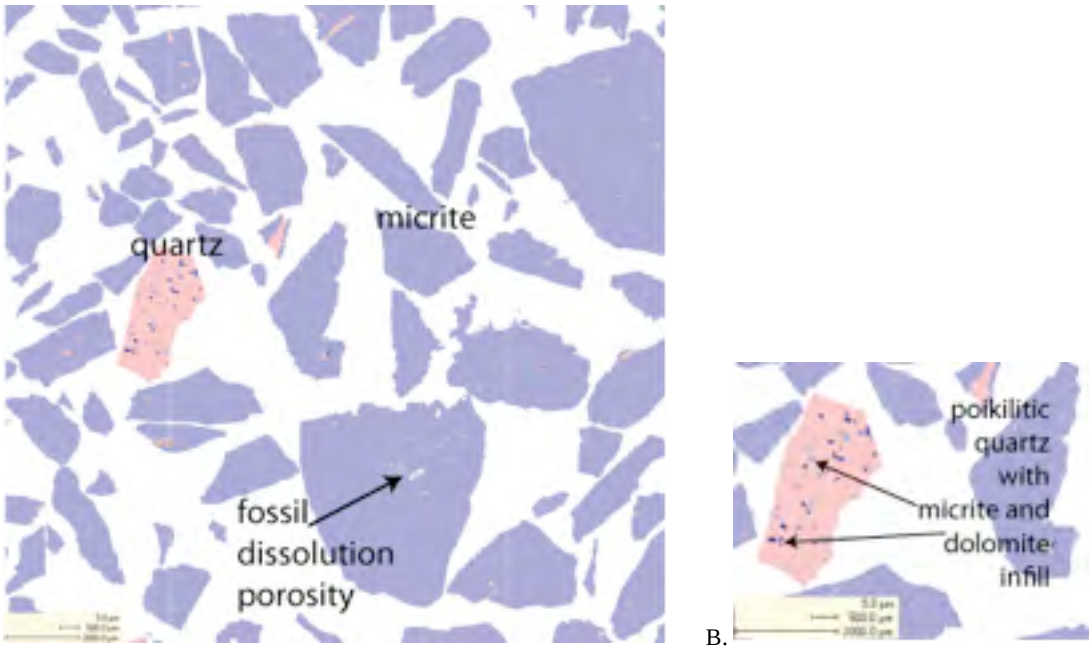

Figure 10: A. Micrite (lime mud) is the dominant lithology in Unit 2 and is composed of numerous tests that are preferentially eroding to produce dissolution porosity. B. Angular poikilitic qaurtz is mechanically infilled by lime mud.

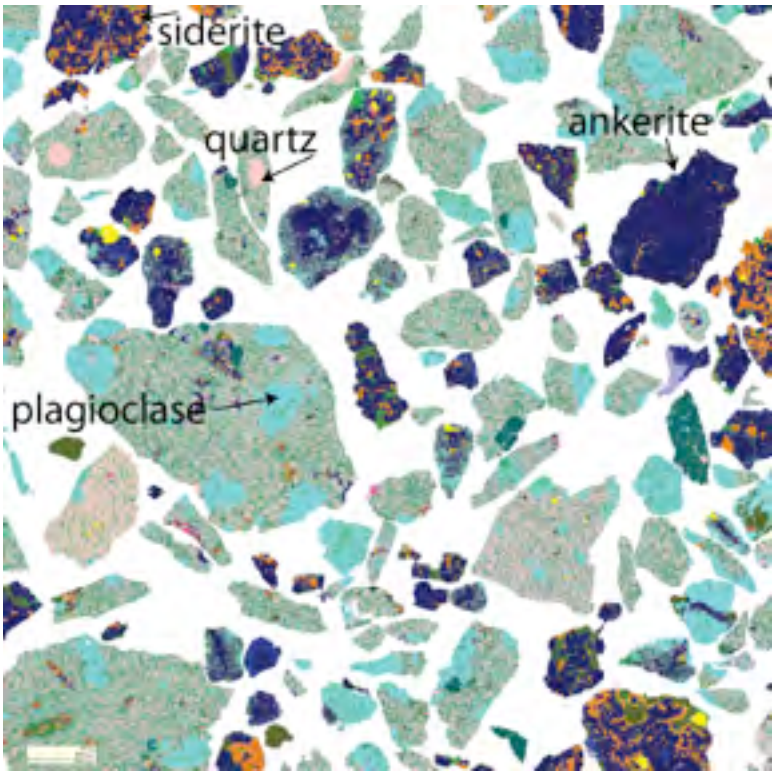

Figure 11: Siliciclastic rock fragments with carbonate/sulfate assemblates (ankerite, siderite, dolomite and pyrite)

6. CONCLUSIONS

McGregor Range is a strategically significant training range for Fort Bliss and other federal agencies in the region. It is somewhat unique in that the range has a relatively modest power demand and with proper planning, could easily provide 100 percent of its own needs. The military refers to this as Net Zero, signifying the ability to avoid using any energy from the public utility grid in the region. While each facility will be different, Fort Bliss has significant renewable energy resources (solar and geothermal). To the extent a functional and economically viable Geothermal or combined geothermal/solar thermal project could be financed and constructed, such a facility would go a long way in helping Bliss meets its Net Zero Energy objective at least for the McGregor Range, if not for the whole base.

While it is too early to determine the exact economic competiveness (cost per KWH) of geothermal power generation at McGregor, the work performed in this project has determined that it is possible to utilize the resource for heating/cooling and possibly even power generation at competitive prices, but additional investment and research will be necessary.

REFERENCES

Finger, J.T. and Jacobson, R.D.: Fort Bliss Exploratory Slimholes: Drilling and Testing, Sandia Report SAND97-3075, (1997), 9.

Fournier, R. O.: Water geothermometers applied to geothermal energy, *Applications of Geochemistry in Geothermal Reservoir Development*, UNITAR-UNDP (ed. F. D'Amore), (1991), 37-69.

Giggenbach, W. F.: Chemical techniques in geothermal exploration, *Applications of Geochemistry in Geothermal Reservoir Development*, UNITAR-UNDP (ed. F. D'Amore), (1991) 119-144.

Henley, R. W., and Ellis, A. J.: Geothermal systems ancient and modern: A geochemical review, *Earth-Science Reviews*, **19**, (1983) 1-50.

Reed, M.H. and Spycher, N. F.: *SOLVEQ: A Computer Program for Computing Aqueous-Mineral-Gas Equilibria*, unpublished manual, 3rd edition, (2006), 1-38.

Reyes, A. G.: Petrology of Philippine geothermal systems and the application of alteration mineralogy to their assessment, *Journal of Volcanology and Geothermal Research*, **43**, (1990), 279-309.